Influence of Power Supplies on the Secondary Arc Test of Solar Arrays

JOURNAL OF SPACECRAFT AND ROCKETS
Vol. 46, No. 3, May–June 2009

Influence of Power Supplies on the Secondary Arc Test of Solar Arrays

Teppei Okumura,* Kazuhiro Toyoda,† and Mengu Cho‡
Kyushu Institute of Technology, Kitakyushu 804-8550, Japan
and
Andreas Kroier§ and Erich Leitgeb¶
Graz University of Technology, Graz, Styria 8010, Austria

DOI: 10.2514/1.40942

A secondary arc test is necessary to improve the design reliability of a solar array. To simulate the power generation of solar arrays, various power supplies are employed for the ground tests. Solar arrays that are illuminated by a light source are the most ideal power supply for the ground test in terms of their impedance. Laboratory experiments were carried out to investigate the appropriateness of a solar array simulator and a current regulative diode power supply for the secondary arc test. There was little difference among the waveforms and the secondary arc duration obtained by a real solar array, the solar array simulator, and the current regulative diode power supply, except the small difference in the rush current at the beginning of the secondary arc and the temporary blackout after the secondary arc. The solar array simulator and the current regulative diode power supply are both acceptable as a power supply for the secondary arc test. The minor difference is associated with the output capacitance of each power supply, which exists even for the real solar array.

Nomenclature

C_L	=	bus capacitance of solar array, F
C_j	=	capacitance of PN junction of solar cell, F
C_k	=	capacitance between a solar cell and substrate, F
C_{out}	=	capacitance of power supply, F
C_1, C_2, C_3	=	string capacitance derived from the equivalent circuit of solar cell networks, F
D_1, D_2, D_3	=	diode
$d_{V\text{sa}}$	=	maximum voltage drop between the cells across the test gap during a secondary arc, V
I_b	=	current waveform; the blowoff current, A
$I_{h_{\text{in}}}$	=	current waveform; the upstream current of solar array coupon, A
$I_{h_{\text{out}}}$	=	current waveform; the downstream current of solar array coupon, A
I_{peak}	=	peak of primary arc current, A
$I_{p_{\text{rush}}}$	=	peak of rush current, A
I_{rush}	=	rush current, A
L_s	=	inductance of solar cell, H
N_p	=	number of electrically independent parallel strings
N_s	=	number of solar cells per string
Q_{rush}	=	charge of rush current, C
R_L	=	load resistance of satellite, Ω
R_s	=	series resistance of solar cell, Ω
R_{sh}	=	parallel resistance of solar cell, Ω
T_{end}	=	end time of primary arc current, s
T_{fall}	=	end time of secondary arc current, s
T_{r1}	=	start time of rush current, s
T_{r2}	=	end time of rush current, s
T_{sus}	=	sustained time of secondary arc, s
V_B	=	voltage waveform; the potential difference between the ground and solar array coupon, V
V_{sa}	=	voltage waveform; the potential difference between the cells cross the test gap, V
V_1	=	power supply voltage to simulate the spacecraft chassis potential, V
V_2	=	power supply voltage to maintain the voltage across the load resistance, V

Received 11 September 2008; revision received 23 January 2009; accepted for publication 26 January 2009.

*Postdoctoral Fellow, Department of Electric Engineering, Tobata-ku; okumura@ele.kyutech.ac.jp.

†Associate Professor, Laboratories of Spacecraft Environment Engineering, Tobata-ku; toyoda@ele.kyutech.ac.jp.

‡Professor, Department of Electrical Engineering, Tobata-ku; cho@ele.kyutech.ac.jp.

§Institute for Broadband Communications, Inffeldgasse 16; andreas.kroier@student.tugraz.at.

¶Associate Professor, Institute for Broadband Communications, Inffeldgasse 16; erich.leitgeb@tugraz.at.

I. Introduction

FOR a modern high-power satellite, to reduce the overall power loss in the power system and its total mass, high-voltage power generation and transmission are necessary [1]. Differential charging due to plasma interaction and subsequent electrostatic discharge (ESD) are critical issues for the safe operation of a high-voltage generating solar array. It is known that ESD between adjacent solar cells can cause a serious problem on the solar array as demonstrated first by the failure of Tempo-2 [1]. To increase the reliability of solar arrays, ESD tests based on correct understanding of the discharge effects on a solar cell are necessary. Currently, an international effort to standardize the solar array ESD test is in progress [2].

A cross-sectional view of a typical solar array is shown in Fig. 1, containing the so-called triple junction, which is the boundary between dielectric (coverglass, adhesive), conductor or semiconductor (interconnector, solar cell), and space. It should be noted here that the word of "triple junction" in the present paper is used with a different meaning from a triple-junction solar cell, that is, InGaP/GaAs/Ge solar cell. To distinguish both of these clearly, InGaP/GaAs/Ge solar cell is called a "multijunction solar cell" in the present paper.

The equilibrium among the fluxes of incoming ions, incoming electrons, and outgoing electrons such as photoelectrons, secondary electrons, and backscattered electrons determines the spacecraft potential in space. In geostationary orbit, the increase of energetic electrons during the substorm is the major cause of spacecraft charging, driving the spacecraft chassis potential to a highly negative potential of the order of kilovolts with respect to the surrounding

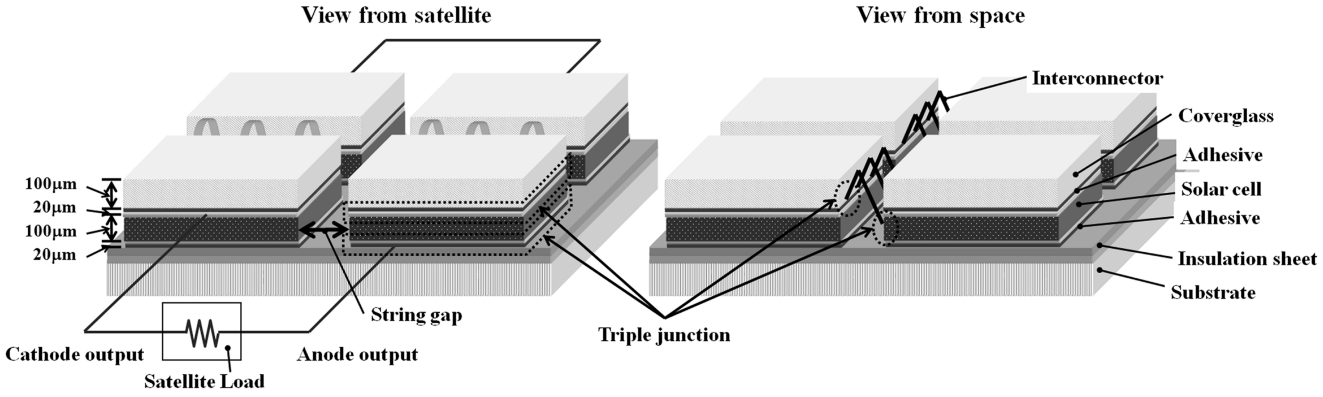

Fig. 1 Cross-sectional view of a typical solar array.

plasma potential. The spacecraft surface insulator may have different potentials from the spacecraft chassis potential, producing the differential charging condition. When the insulator potential is more negative than the chassis, it is called the normal potential gradient. When the insulator is more positive, it is called the inverted potential gradient. The inverted potential gradient is paid more attention in terms of solar array ESD, because the high secondary electron coefficient of coverglass makes its potential more positive than the solar cell for most of the charging environment in space [3] and the ESD inception threshold is on the order of hundreds of volts [4] compared to the threshold on the order of kilovolts for the case of normal potential gradient [5]. Under the inverted potential gradient, a discharge occurs due to the electric field concentration at the triple junction [6]. This discharge is called primary ESD or primary arc (PA) [2].

Normally, adjacent solar cells have a potential difference on the solar array circuit (see the string gap in Fig. 1). The generated voltage determines the value of the potential difference. In the case of a typical commercial telecommunication satellite with a 100 V bus, the potential difference at the string gap is as high as 100 V. The highly conductive plasma short-circuits the string gap when a primary arc occurs there. This event is called a secondary arc [7]. Because the power of the secondary arc comes from the solar array, the power from the arced solar array string is lost for the duration of the secondary arc. In the worst case, when the string circuit is permanently short-circuited, power is permanently lost.

Currently, research institutes and satellite manufacturers perform ESD tests before launch to check whether the solar array is protected from secondary arcs [4,5]. Because it is unrealistic to test the entire solar array paddle in the ground test, only a part of the array, often called a coupon panel, is used for the test. It is necessary to simulate the solar array circuit and the generated power by using external power supplies and electric circuits. The ideal power supply is an illuminated solar array.

In an ESD test, however, the power supply is often required to provide various sets of output voltage and current, which is not an easy task for a real solar array. A real solar array also requires a high-power light source that simulates the light spectrum well in orbit. Therefore, a real solar array is not realistic as the power supply for an ESD test and an alternative power supply is usually used. A commercial solar array simulator (SAS) has been most commonly used all over the world [8,9]. Payan et al. [10] compared the current waveforms provided by an ordinary dc power supply and a SAS and demonstrated that the ordinary power supply was not suitable for solar array ESD tests because of its large output capacitance. Toyoda et al. [11] proposed a power supply which consisted of current regulative diodes (CRD). The key points in selecting the power supply for an ESD test is the inherent capacitance and response time. Despite the previous works, there has been no effort to compare the output of the alternative power supplies to the one of the illuminated solar array.

The purpose of the present paper is to evaluate how well the SAS and CRD methods represent flight conditions in view of the generation of the secondary arc phenomenon. In the present paper, we carry out a laboratory test of solar array secondary arc and compare the arc waveform and the arc duration obtained from the SAS and CRD with the waveform and the duration obtained from an illuminated solar array. The second part of this paper describes the test setups. Basically, we kept everything the same except the power supplies in the test circuit. The third part discusses the experimental results. In the fourth part, we conclude the paper with suggested future works.

II. Electrostatic Discharge Test

A. Test Coupon

The test coupon is shown in Fig. 2. It is made of silicon solar cells of 35 × 70 mm each with an integrated bypass function. Coverglass is glued onto each cell. Twelve silicon cells are glued on the aluminum honeycomb carbon fiber reinforced plastic (CFRP) panel by a room temperature vulcanization (RTV) silicon adhesive. The substrate is covered by a polyimide sheet. Because the four silicon cells are connected in series, there are three strings in the coupon.

For the ESD test, string B and string C were used. All the triple-junction points were insulated by the polyimide tape, except for the string gap between string B and string C. The bus bars were insulated

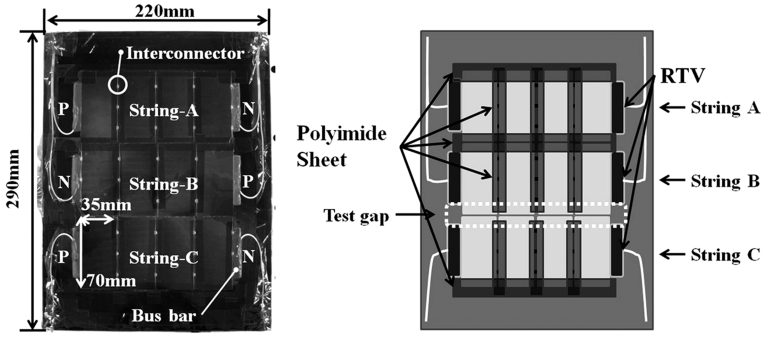

Fig. 2 Solar array coupon and the gap for secondary arc test.

by the silicon adhesive. The insulation part on the solar array coupon is also shown in Fig. 2. We exposed only the gap between the strings to avoid unnecessary primary arcs at the other points, as the purpose of the experiment was to compare the three power supplies in case of secondary arcs at the gap, not to investigate the strength of the coupon against secondary arc. Therefore, this design is not recommended for real a flight panel, where primary arcs at the string gaps should be avoided to suppress the secondary arcs.

B. Experimental System

The experimental system is shown in Fig. 3. The size of the vacuum chamber is 1 m in length and 1.2 m in diameter. During the test, the pressure was approximately 2.4×10^{-3} Pa. An electron cyclotron resonance (ECR) plasma source generates xenon plasma inside the vacuum chamber. With a 0.4 sccm gas flow, the plasma density was 2×10^{12} m^{-3} and the electron temperature was 1 eV [12]. The use of the plasma source was merely to produce the inverted potential gradient on the solar array coupon. There are reports that there is little difference in the results of the secondary arc test [13] between the more geostationary-orbit-like experiment using an electron beam to charge the solar array coverglass and the low-Earth-orbit-like experiment using a low-temperature plasma source like the one used in the present paper. The main purpose of the present paper is to compare the three types of power supplies, keeping the other experimental parameters identical. Therefore, the selection of the charging method does not matter for the present case as long as the inverted potential gradient is produced. The waveform data acquisition system consists of a high-speed 8-bit data acquisition board and a commercial PC to store the current and voltage waveforms during the test. This system can simultaneously calculate the peak current, charge, and duration of the primary arc. It can also send a trigger signal to the image acquisition system when a primary arc is detected. The image acquisition system identifies the primary arc position from the video image taken by a charge-coupled device (CCD) camera during the test. The discharge images are stored on a hard disc drive (HDD).

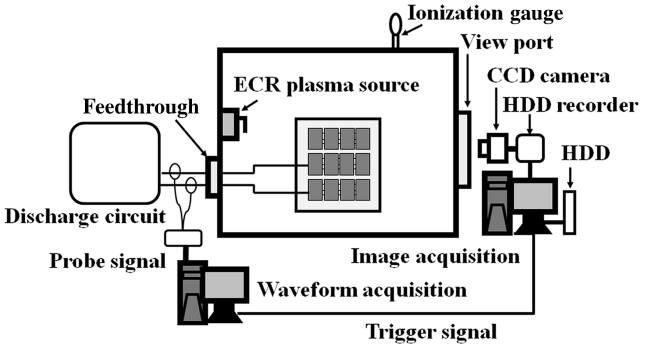

Fig. 3 Experimental system.

C. Discharge Circuit

The discharge circuit, including the solar array, is shown in Fig. 4. To use the solar array as a power supply, a metal-halide lamp is used to irradiate the solar array (part 1).

The external power supply solar array coupon is shown in Fig. 5. The external power supply solar array coupon consists of 50 InGaP/GaAs/Ge solar cells, the so-called multijunction (MJ) cell. To use the solar array for the secondary arc test as a power supply, fifty multijunction cells are connected in series. In the present paper, we call the solar array a MJ array. The power generation system, which consists of the solar array and metal-halide lamp, is shown in Fig. 6. The spectrum of the metal-halide lamp ranges from 350 to 700 nm. The intensity is highest in the visible light wavelength. The reflection panels are deployed on the rear, right, and left sides of the lamp holder to avoid light scattering. Fans keep the temperature of the solar array surface to approximately 80 °C while it is illuminated. The open-circuit voltage did not change for less than 1 h which was the maximum illuminated time. The light current-voltage characteristic (light I-V) of the MJ array is shown in Fig. 7. The open-circuit voltage is 120 V and the short-circuit current is 0.5 A, not so much different from the air mass zero (AM0) condition, because the open-circuit voltage of one multijunction cell is 2.5 V in the air mass zero condition (a single multijunction cell has the open-circuit voltage of 2.5 V and the short circuit of 0.5 A). However, the fill factor of the MJ array is not as good as the expected fill factor at AM0 because the light spectrum of the metal-halide lamp was not similar to the AM0 spectrum. Although the fill factor of the MJ array is not as good as AM0, the metal-halide lamp system can still supply enough light intensity for the MJ array to generate the electricity necessary for the secondary arc test. The most important thing in this experiment is the impedance of the power supply. In that sense, matching the fill factor of the MJ array to the AM0 condition is not critical. Therefore, the MJ array shown in Fig. 5 is applicable for the secondary arc test. The positive (P) electrode of the MJ array is connected to the P electrode of the coupon inside the chamber. The negative (N) electrode of the MJ array is similarly connected to the N electrode of the coupon. Because the coupon inside the chamber is not illuminated (dark condition), to supply the current in the forward direction of a solar cell as a diode, the coupon should be connected as described herein. The coupon inside the chamber is made of crystalline silicon solar cells, not the MJ solar cell. Because the main purpose is to compare the external power supplies, what type of solar cells we use for the test coupon is minimally important.

Part 2 in Fig. 4 simulates the electrical load of a spacecraft. R_L is the load resistance and C_L represents the bus capacitance. The voltage difference over the string gap can be controlled by changing R_L. The

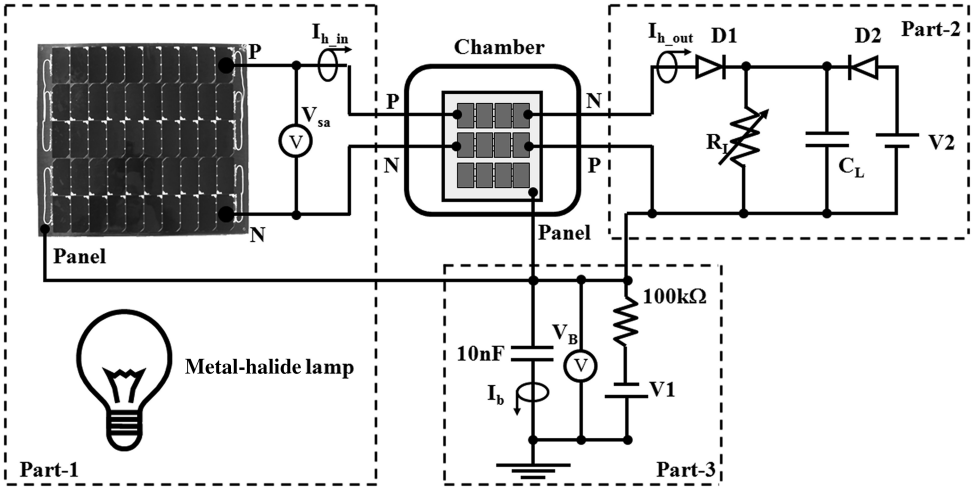

Fig. 4 Discharge circuit with solar array.

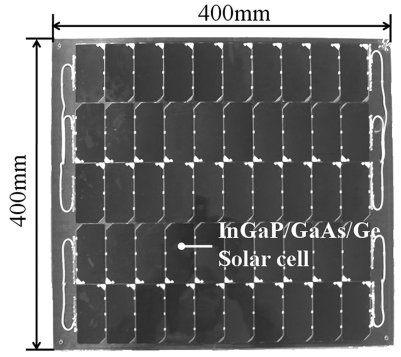

Fig. 5 External power supply solar array coupon; MJ array.

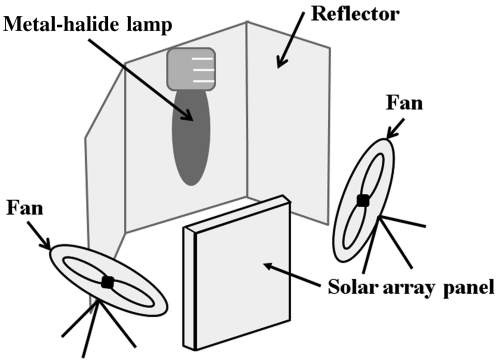

Fig. 6 Metal-halide lamp system.

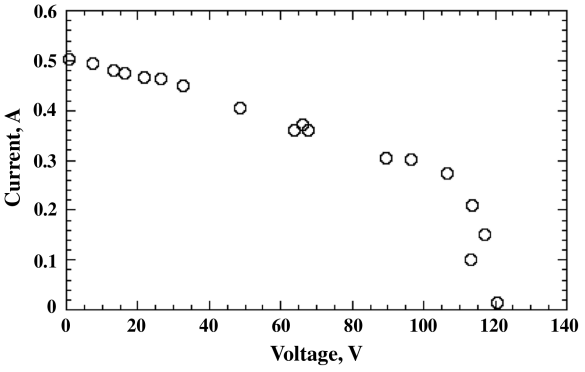

Fig. 7 Light current-voltage characteristics of solar array.

voltage across the resistance R_L is slightly higher than the voltage V_2. Therefore, before a secondary arc occurs, the diode D_1 is open and the diode D_2 is closed. Then the current to R_L is provided by the MJ array. Once a secondary arc occurs, a fraction of the current from the MJ array goes to the arc plasma. The slight decrease of the current to R_L leads to the decrease of the voltage across R_L. Once it becomes less than V_2, the diode D_2 becomes open and the voltage across the resistance is maintained at V_2. Then the diode D_1 is closed, directing all the current from the MJ array to the arc plasma. We can recognize the secondary arc inception from the waveform measured at $I_{\mathrm{hot}_{\mathrm{out}}}$ because the current drops to zero during the secondary arc at $I_{\mathrm{hot}_{\mathrm{out}}}$. The secondary arc waveform is measured by the current probes (dc to 50 MHz) at $I_{h_{\mathrm{in}}}$ and $I_{h_{\mathrm{out}}}$. To measure the potential difference at the string gap during a secondary arc, the differential voltage probe (dc to 25 MHz) V_{sa} was used. Because of the accuracy of the differential voltage probe, measurement error is approximately 8 V.

Part 3 in Fig. 4 reproduces the spacecraft potential against the ambient space plasma. The power supply V_1 simulates the spacecraft potential. The polarity of V_1 is negative to generate the inverted potential gradient on the coupon. By varying V_1, we can control the primary arc frequency. In the case of the secondary arc test with illuminated solar array, V_1 ranges from -650 to -850 V. In the case of SAS and CRD, V_1 is set at -850 and -1050 V, respectively. The polarity of V_1 is chosen to produce the inverted potential gradient condition. In a typical ESD test on solar array, the capacitance connected in parallel with V_1 simulates the capacitance of spacecraft structure to the ambient space and the capacitance of the solar array coverglass that cannot be housed inside the vacuum chamber. The realistic value of the capacitance is still a matter of controversy. For the present work, we selected the value of 10 nF for the following two practical reasons. We wanted to cause the least damage to the coupon by avoiding a large value. At the same time, we wanted to have a large enough capacitance to cause the optical flash detectable by the video to identify the primary arc location. A resistance of 100 kΩ is connected in series with V_1. This resistance prevents V_1 from supplying the current to the chamber via primary arc plasma during primary arc. The resistance R_L is usually determined from the viewpoint of the maximum current provided by the power supply. For example, for a bias voltage of 1 kV, the resistance of 100 kΩ limits the current to 0.01 A, negligible compared to the arc current.

The discharge circuit with CRD or SAS is shown in Fig. 8. Part 4 in Fig. 8 corresponds to part 1 in Fig. 4. Payan et al. [10] proposed the discharge circuit shown in Fig. 8. The capacitances C_1, C_2, and C_3 simulate the capacitances of the solar array. C_1 and C_3 are defined as in Eq. (1), and C_2 is defined as in Eq. (2) [10]:

$$C_1 = C_3 = N_p \sqrt{C_j C_k}\,\frac{1}{\tanh[(N_s/2)\sqrt{C_k/C_j}]} \tag{1}$$

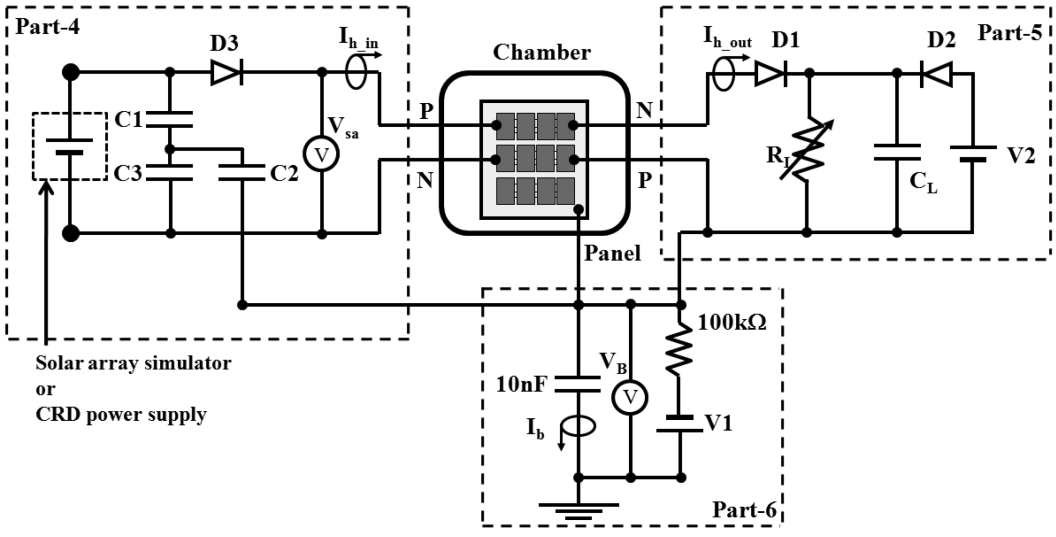

Fig. 8 Discharge circuit with CRD power supply or solar array simulator.

Table 1 Condition of the power supply in the solar array, SAS, and CRD power supply

	Output voltage, V	Output current, A	R_L, Ω	V_1, V
MJ array	87	0.32	272	−650 to −850
SAS	92	0.30	306	−850
CRD	87	0.28	310	−1050

$$C_2 = N_p \sqrt{C_j C_k}\sinh(N_s \sqrt{C_k / C_j}) \tag{2}$$

We set $C_j = 600$ nF assuming the capacitance of a PN junction of a multijunction cell. The capacitance of the adhesive and the insulation sheet below a solar cell C_k is 400 pF, assuming the dielectric constant of 2.5 and 3.5 and the thickness of 100 and 50 μm for the adhesive and the insulation sheet, respectively [13]. Then, Eqs. (1) and (2) give $C_1 = 27$ nF, $C_2 = 26$ nF, and $C_3 = 27$ nF. The number of solar cells that are connected in series N_s is 50 and the number of the string N_p is unity. To protect the power supply, a diode D_3 is connected in series to the power supply.

Part 5 and part 6 are equal to part 2 and part 3 in Fig. 4. The output voltage, the output current, R_L, and V_1 for all three methods are listed in Table 1. There is an error of 8 V at maximum in the output voltages listed in Table 1 associated with the use of a 500X differential high-voltage probe for V_{sa}. Because the secondary arc inception probability depends on the voltage across the string gap, the output voltage and the output current of power supplies are equally set in all three cases: MJ array, SAS, and CRD. Therefore, the influence of the power supply on the secondary arc test can be compared. Additionally, the output current of power supply, that is, string current in the solar array, affects the sustained time of secondary arc. The larger string current can cause a longer secondary arc as reported in various previous works [13–16]. We used the output current of 0.3 A throughout the present work. By limiting the current to such a small value, we can minimize the risk of damaging the coupon so that we can use the same coupon for the tests using different power supplies.

III. Experiment Result

We categorize a secondary arc by its duration (see Fig. 9). The primary arc is the current provided by I_b in the present test setup. The current is mainly provided by the external capacitance (10 nF). The nonsustained arc (NSA) represents a secondary arc where the string gap is short-circuited and the current of $I_{h_{out}} - I_{h_{in}}$ flows through the arc plasma while the PA current continues. NSA, however, ends as the PA ends. The temporary sustained arc (TSA) is a secondary arc where the short circuit continues even after the end of PA but then ceases spontaneously. For the present paper, we set lasting for more than 2 μs after the end of PA as the judging criteria of TSA from NSA. The limit of 2 μs was chosen to safely distinguish TSA from NSA against the oscillation at the end of the arc current. The permanent sustained arc (PSA) represents a secondary arc where the short circuit continues until the power supply is intentionally turned off. Once a PSA occurs at the string gap, the conductive substrate below the insulation sheet, such as CFRP honeycomb, is exposed due to carbonization of the insulation sheet by the arc plasma. Then the solar array can no longer provide power to the spacecraft load because the string current is bypassed via the conductive substrate. In the cases of a NSA or a TSA, the spacecraft load loses the power only for the duration of the short circuit of the string gap.

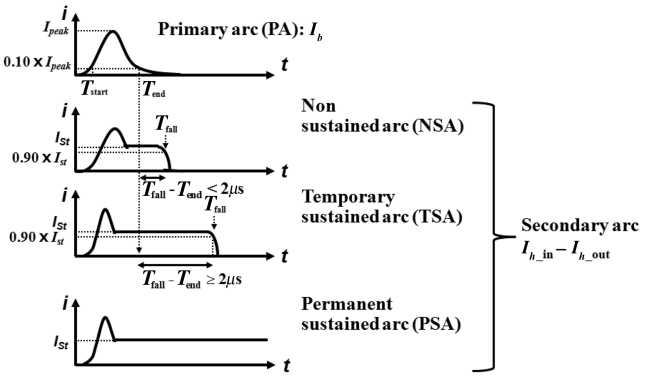

Fig. 9 Secondary arc definition.

The waveforms of the primary arcs are measured by the current probe I_b in Fig. 4. The current waveforms are measured by the current probes $I_{h_{in}}$ and $I_{h_{out}}$, and the secondary arc current is derived from Eq. (3):

$$\text{secondary arc current} = I_{h_{in}} - I_{h_{out}} \tag{3}$$

The end time T_{end} is defined as the time when I_{peak} becomes 10% of its peak value. The duration of the secondary arc is defined as the time from T_{end} to the time when the arc current becomes 90% of the output current of the power supply T_{fall}. The time duration of secondary arc T_{sus} is obtained from Eq. (4):

$$T_{sus} = T_{fall} - T_{end} \tag{4}$$

The waveforms of a PA, a TSA, $I_{h_{in}}$, $I_{h_{out}}$, and V_{sa} in the case of a secondary arc test with a MJ array are shown in Fig. 10. Because the string gap is short-circuited for 3.7 μs after the PA, the discharge

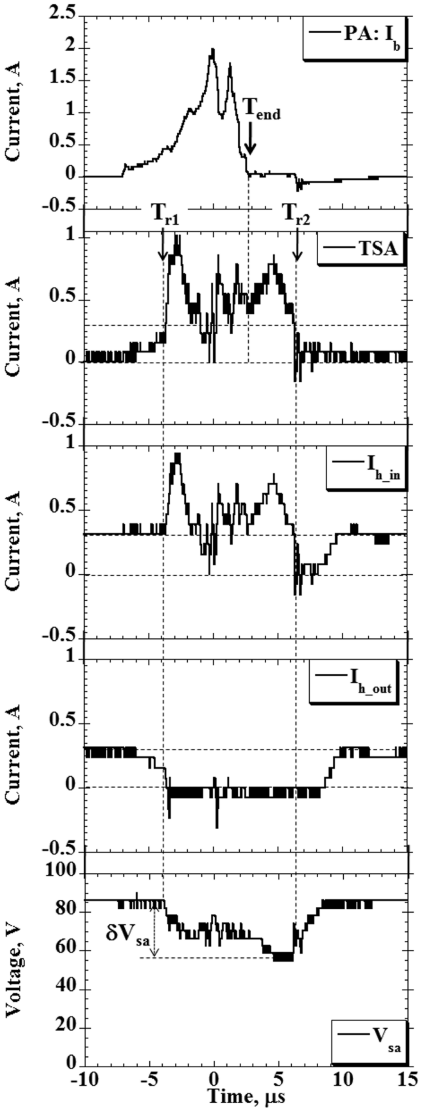

Fig. 10 Typical current waveform and voltage waveform during temporary sustained arc in the case of the MJ array.

event shown in Fig. 10 is a TSA. During the experiment, 112 TSAs occurred with the MJ array as a power supply. We note that, after the secondary arc inception, the current $I_{h_{in}}$ becomes more than 0.3 A provided by the MJ array, which we call rush current in the present paper, and drops to a zero for several microseconds after the end of TSA. This tells us that there is a capacitance between the location of the current probe measuring $I_{h_{in}}$ and the MJ array. In Fig. 10, the capacitance of the MJ array discharged as V_{sa} dropped from 85 to 60 V during TSA producing the rush current. After the TSA, the current from the MJ array were used to recharge the capacitance while the voltage V_{sa} recovered to 85 V, causing the temporary blackout from $t = 6$ to 8 μs. A typical equivalent circuit of a solar cell is shown in Fig. 11. I_{sc} is light electron current. C_j is the capacitance associated with the PN junction mentioned in Sec. II. This C_j is probably responsible for the capacitance of the MJ array.

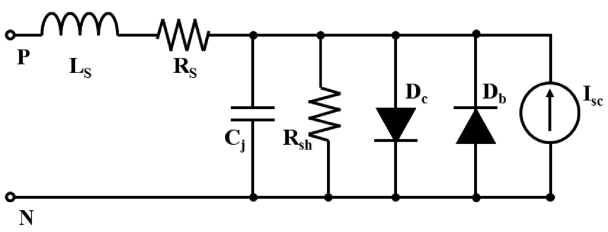

Fig. 11 Solar cell equivalent circuit.

Figure 12 shows the same waveforms for the SAS case. Again, the arc shown here is a TSA (6.2 μs after PA). In this case, 14 TSAs occurred. Figure 13 shows the waveforms for the case of the CRD power supply. The arc is also a TSA (3.2 μs after PA). Four TSAs occurred with CRD as a power supply. Comparing Figs. 10, 12, and 13, we can see there is no significant difference among the three power supplies. The rush current at the beginning of the secondary arc inception and the temporary blackout of $I_{h_{in}}$ after the end of TSA are also seen in Figs. 10 and 12. There is a ringing after the end of TSA in Figs. 12 and 13, for which the cause is not known yet. The TSA durations for the cases of the MJ array, the SAS, and the CRD are listed in Table 2. We note that the TSA duration is almost the same for the different power supplies. The overall conclusion from the comparison of Figs. 10, 12, and 13 is that we can use either SAS or CRD as a substitute for the real solar array in a secondary arc test.

The output capacitances of the three power supplies can be estimated from the waveform at $I_{h_{in}}$. To calculate the rush current waveform, the output current of the power supply is subtracted from the waveform of $I_{h_{in}}$. For the case of the MJ array, the output current varies depending on V_{sa} according to the I-V characteristic shown in Fig. 7. The output current can be approximated by the following equation:

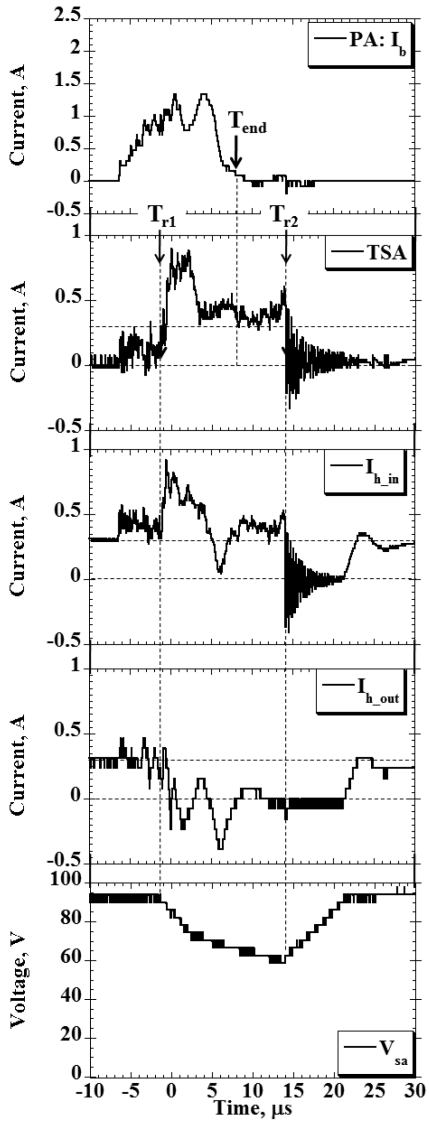

Fig. 12 Typical current waveform and voltage waveform during temporary sustained arc in the case of solar array simulator.

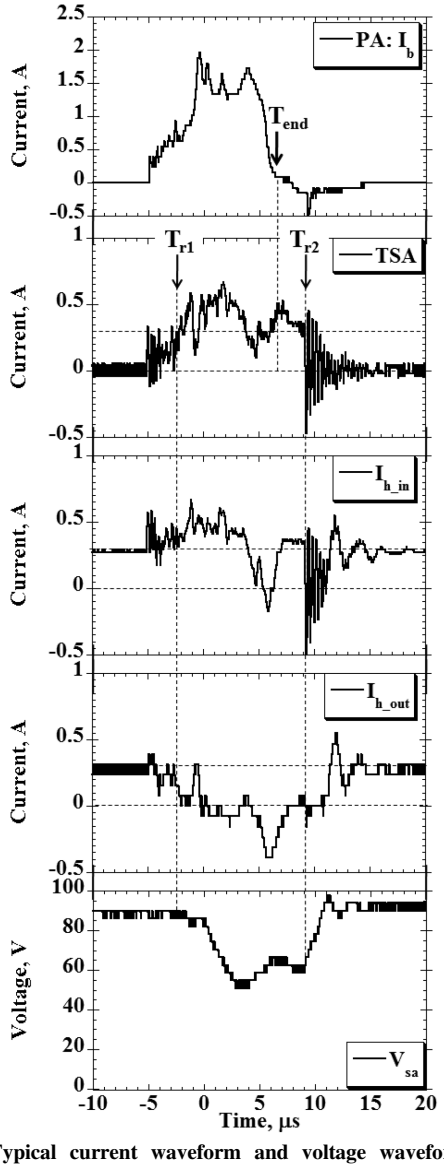

Fig. 13 Typical current waveform and voltage waveform during temporary sustained arc in the case of current regulative diode power supply.

Table 2 Comparison of arc duration with different power supplies, average, and standard deviation

	Arc duration, T_{sus}, μs			
	Minimum	Maximum	Average	Number of arc
MJ array	2.1	8.1	4.1 ± 1.7	112
SAS	2.5	7.2	4.9 ± 1.5	17
CRD	3.2	7.1	4.9 ± 1.4	4

Table 3 Output capacitance, average, and standard deviation

	Q_{rush}, μC	C_{out}, nF
MJ array	1.0 ± 0.4	57 ± 20
SAS	2.4 ± 0.5	81 ± 17
CRD	0.4 ± 0.1	13 ± 9

$$I = -0.0021 \times V + 0.499 \tag{5}$$

We substituted the voltage measured as V_{sa} into Eq. (5) and calculated the output current from the solar array. The output current is subtracted from the current measured at $I_{h_{in}}$ to derive the rush current I_{rush}. For the cases of CRD and SAS, 0.3 A are subtracted from $I_{h_{in}}$.

The peak of the rush current is defined as $I_{p_{rush}}$. The moments when the current becomes 5% of $I_{p_{rush}}$ are indicated by T_{r1} and T_{r2}. The charge of the rush current Q_{rush} is calculated from Eq. (6):

$$Q_{rush} = \int_{Tr1}^{Tr2} I_{rush}(t)\,dt \tag{6}$$

The magnitude of the variation of the output voltage during a TSA is defined as δ_{Vsa}. Here, the output capacitance of the power supply C_{out} is defined as in Eq. (7):

$$C_{out} = \frac{Q_{rush}}{\delta V_{sa}} \tag{7}$$

In Table 3, Q_{sp} and C_{out} are shown for the cases of the MJ array, the SAS, and the CRD. For the cases using the SAS and the CRD, C_1, C_2, and C_3 are connected in parallel to the SAS/CRD. Therefore, C_{out} listed in Table 3 indicates the total capacitance of the capacitances, including the power supply and C_1, C_2, and C_3.

Figure 14 shows a part of the discharge circuit (shown in Fig. 8). In the cases of the SAS and the CRD, C_1, C_2, and C_3 are connected to C_{out} in parallel. To measure the total capacitance of C_1, C_2, and C_3 an inductance capacitance resistance meter was connected to node 1 and node 2 instead of the power supply. Because there is no secondary arc current flowing into part 5 and part 6 in Fig. 8, those parts can be ignored. The total capacitance of the circuit shown in Fig. 14 is 15 nF in dark condition. Therefore, the inherent output capacitance of SAS and CRD is more than 66 nF and less than 1 nF, respectively. (We used Agilent 4351B as the SAS, which is said to typically have an output capacitance of 50 nF.)

Although the difference in the output capacitance found in the present paper was not large enough to affect the result of secondary arc duration nor the overall picture of the waveforms, it is always desirable to have the exact match to prepare for the case where the output capacitance of the real solar array strings becomes important. Table 3 shows that the capacitance of the MJ array is closer to the total capacitance of the SAS than that of the CRD. However, this is just coincidence because C_1, C_2, and C_3 for the SAS and the CRD are not calculated considering the capacitance of the power supply. If the size of the MJ array changes, the capacitance C_{out} of the MJ array also changes. When we determine C_1, C_2, and C_3, we have to take into account the inherent capacitance of the SAS or the CRD. Because the inherent capacitance of the CRD is much smaller than that of the SAS, the CRD method has more flexibility to match the real solar array.

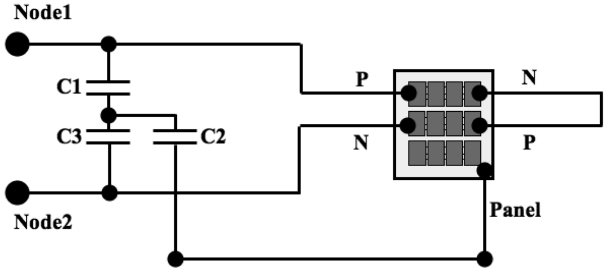

Fig. 14 The total capacitance of C_1, C_2, C_3, and sample.

IV. Conclusions

To investigate the influence of power supplies on the results of secondary arc tests, experiments were performed with the SAS, the CRD, and multijunction arrays illuminated by a spotlight.

The MJ solar array is the most realistic power supply for the secondary arc test in terms of the inherent impedance of the power supply. A comparison of the TSA durations among the different types of power supplies showed no variance. There was no significant difference in the current waveform among the three power supplies. Therefore, either the SAS or the CRD is acceptable for the secondary arc test.

The experiment with the MJ array showed that there was a capacitance connected in parallel to the solar array output. The capacitance is discharged during a secondary arc; therefore, the secondary arc current becomes larger than the short-circuit current of a solar array. To charge the capacitance after a secondary arc, the solar array output shows a temporary blackout. The output capacitance existed in the other two power supplies. They were all less than 100 nF: not large enough to affect the test results. When the inherent capacitance of the solar array circuit becomes large, however, care should be taken to match the capacitance of a substituting power supply to the one of the solar array, as the rush current may affect the test result. In addition, the solar array also has inductance and resistance. As a future task, we will study the method to obtain the accurate impedance of the solar array.

Acknowledgment

This research was carried out as an International Joint Research Program (05IS084) supported by the New Energy Industrial Comprehensive Development Organization of Japan.

References

[1] Katz, I., Davis, V. A., and Snyder, D. B., "Mechanism for Spacecraft Charging Initiated Destruction of Solar Arrays in GEO," *36th Aerospace Science Meeting*, AIAA Paper 98-1002, 1998.

[2] Cho, M., "Status of ISO Standardization Efforts of Solar Panel ESD Test Methods," *10th Spacecraft Charging Technology Conference on Disk* [CD-ROM], Japan Aerospace Exploration Agency, Tsukuba, Japan, 2007.

[3] Cho, M., Kawakita, S., Nakamura, M., Takahashi, M., Sato, T., and Nozaki, Y., "Number of Arcs Estimated on Solar Array of a Geostationary Satellite," *Journal of Spacecraft and Rockets*, Vol. 42, No. 4, 2005, pp. 740–748. doi:10.2514/1.6694

[4] Cho, M., Ramasamy, R., Matsumoto, T., Toyoda, K., Nozaki, Y., and Takahashi, M., "Laboratory Tests on 110V Solar Arrays in a Simulated Geosynchronous Orbit Environment," *Journal of Spacecraft and Rockets*, Vol. 40, No. 2, 2003, pp. 211–220. doi:10.2514/2.3955

[5] Cho, M., Kim, J., Hosoda, S., Nozaki, Y., Miura, T., and Iwata, T., "Electrostatic Discharge Ground Test of a Polar Orbit Satellite Solar Panel," *IEEE Transactions on Plasma Science*, Vol. 34, No. 5, Oct. 2006, pp. 2011–2030. doi:10.1109/TPS.2006.881935

[6] Hastings, D., and Garrett, H., *Spacecraft Environment Interactions*, Cambridge Univ. Press, Cambridge, MA, 1996, pp. 142–198.

[7] Levy, L., Sarrail, D., Viel, V., Amorim, E., Serrot, G., and Bogus, K., "Secondary Arcs on Solar Arrays: Occurrence, Threshold, Characteristics and Induced Damage," *7th Spacecraft Charging Technology*

Conference on Disk [CD-ROM], ESA, Noordwijk, The Netherlands, April 2001.

[8] Berthou, C., Boulanger, B., and Levy, L., "Plasma ESD Qualification Test Procedure of Alcatel Alenia Space Solar Array," *IEEE Transactions on Plasma Science*, Vol. 34, No. 5, Oct. 2006, pp. 2004–2010. doi:10.1109/TPS.2006.883371

[9] Vayer, B., Furguson, D., and Galofaro, J., "Detrimental Effect of Arcing on Solar Array Surfaces," *10th Spacecraft Charging Technology Conference on Disk* [CD-ROM], Japan Aerospace Exploration Agency, Tsukuba, Japan, June 2007.

[10] Payan, D., Schwander, D., and Catani, J. P., "Risks of Low-Voltage Arcs Sustained by the Photovoltaic Power of a Satellite Solar Array During an Electrostatic Discharge. Solar Arrays Dynamic Simulator, Spacecraft Charging Technology," *Proceedings of the 7th Spacecraft Charging Technology Conference*, ESA, Noordwijk, The Netherlands, April 2001, pp. 447–453.

[11] Toyoda, K., Aso, S., Kyoku, T., Kitamura, T., and Cho, M., "Proposal of a Current Regulative Diode for Power Supply in Sustained Arc Test," *IEEE Transactions on Plasma Science*, Vol. 34, No. 5, 2006, pp. 1967–1972.
doi:10.1109/TPS.2006.881933

[12] Hayashi, H., Saionji, A., Toyoda, K., Cho, M., and Kuninaka, H., "Development of Plasma Interaction Acceleration Test Facility for Study on Space Material Deterioration," *23rd International Symposium on Space Technology Science*, ISTS-2002-b-28, 2002.

[13] Kitamura, T., Masui, H., Toyoda, K., and Cho, M., "Secondary Arc Tests on Solar Array for International Standardization of ESD Test and Japanese Spacecraft Charging Guideline," *10th Spacecraft Charging Technology Conference on Disk* [CD-ROM], Japan Aerospace Exploration Agency, Tsukuba, Japan, June 2007.

[14] Levy, L., Sarrail, D., Amorim, E., Serrot, G., Bogus, G., "Secondary Arcs on Solar Arrays: Occurrence, Thresholds, Characteristics and Induced Damage," *7th Spacecraft Charging Technology Conference on Disk* [CD-ROM], ESA, Noordwijk, The Netherlands, April 2001.

[15] Amorim, E., Levy, L., Vacquie, S., Gardou, J-P., and Bogus, K., "Vacuum Arcs: Literature Review and Common Characteristics with Secondary Arcs on Solar Arrays," *7th Spacecraft Charging Technology Conference on Disk* [CD-ROM], ESA, Noordwijk, The Netherlands, April 2001.

[16] Lafferty, J.-M., *Vacuum Arcs: Theory and Application*, Wiley, New York, 1980.

I. Boyd
Associate Editor